

A constitutive law for cross-linked actin networks by homogenization techniques

Denis Caillerie^a, Karin John^b, Chaouqi Misbah^b, Philippe Peyla^b, Annie Raoult^c

^a*L3S-R, BP 53 - 38041 Grenoble Cedex 9, France*

^b*LSP UMR 5588, Université J. Fourier and CNRS, BP 87 - 38402 Grenoble Cedex, France*

^c*Laboratoire MAP5 UMR 8145, Université Paris Descartes, 45 rue des Saints Pères, 75270 Paris Cedex 06, France*

Abstract

Inspired by experiments on the actin driven propulsion of micrometer sized beads we develop and study a minimal mechanical model of a two-dimensional network of stiff elastic filaments grown from the surface of a cylinder. Starting out from a discrete model of the network structure and of its microscopic mechanical behavior we derive a macroscopic constitutive law by homogenization techniques. We calculate the axisymmetric equilibrium state and study its linear stability depending on the microscopic mechanical properties. We find that thin networks are linearly stable, whereas thick networks are unstable. The critical thickness for the change in stability depends on the ratio of the microscopic elastic constants. The instability is induced by the increase in the compressive load on the inner network layers as the thickness of the network increases.

The here employed homogenization approach combined with more elaborated microscopic models can serve as a basis to study the evolution of polymerizing actin networks and the mechanism of actin driven motion.

Keywords: A-microstructure, B-biological material, B-constitutive behavior, C-stability and bifurcation, homogenization

2010 MSC: 74Q05, 74Q15

1. Introduction

Dynamic filamentous polymer networks play an essential role in the mechanics of living cells. However, adequate constitutive equations, which take into account the growth history of the networks and the thereby developing prestresses, are difficult to obtain. One prominent example, which shall serve as a starting point for this paper, is the actin filament network. Actin filaments cross-linked by a special protein complex

Email addresses: denis.caillerie@hmg.inpg.fr (Denis Caillerie),
karin.john@ujf-grenoble.fr (Karin John), chaouqi.misbah@ujf-grenoble.fr
 (Chaouqi Misbah)

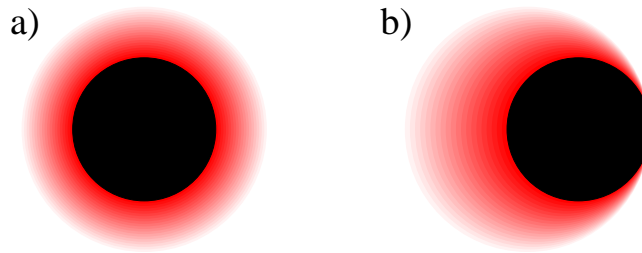


Figure 1: The actin network (shades in red) grows initially in a symmetric cloud (a) from a bead surface (black) until a spontaneous symmetry breaking occurs and the growth continues in an asymmetric fashion (b). Newer (older) network layers are in dark (light) red.

called Arp2/3 complex¹ play a key role in cell motility [1] as well as in the motion of cellular organelles [2] or pathogens [3, 4] inside their respective host cells.

This actin driven motion has been reconstituted under minimal conditions [1] using beads [5], vesicles [6], and droplets [7]. The basic biochemical processes necessary for motion are by now well characterized (for a review see [8] and references therein). Briefly, under the action of several auxiliary proteins, actin polymerizes into a polar filament network, whereby filament elongation and filament linkage are restricted to a zone close to the surface of the propelled object, i.e. the internal interface (The filament network is highly porous and does not hinder the diffusion of monomers to the surface of the object.). Depolymerization takes place far away from the object, i.e. at the external interface. Therefore, new network material is inserted between the already existing network and the object and forces the older network away from the object [see Fig. 1 (a)]. If this type of growth is occurring on curved surfaces, the network experiences large stresses and deformation as growth proceeds. In experiments with actin-propelled biomimetic objects (e.g. beads) [5, 6, 7] it was shown, that initially the actin networks forms a symmetrical cloud around the object, until a spontaneous symmetry-breaking occurs [see Fig. 1 (b)]. Then the network is growing faster on one side than on the other and finally the object starts to move pushed by an actin comet. Thereby actin is continuously polymerizing in the contact region between the bead and the comet.

Thus the (chemical) out-of-equilibrium process of polymerization/depolymerization (which is nevertheless stress dependent, see [9] and references therein) and the action of enzymes produce a network in a pre-stressed state, which does not relax on the timescale of symmetry-breaking and which depends on the history of growth [5, 10, 11, 12]. Several theoretical studies have addressed this problem either using discrete [5, 13] or phenomenological continuous models [14, 15, 16] without, however, obtaining an adequate constitutive law for the network. A type of homogenization model has

¹The Arp2/3 complex is a special protein complex which induces the nucleation of new actin filaments at already existing ones, thus triggering the formation of Y-junctions. It is activated by other enzymes (e.g. ActA, Wasp) which are bound to the membrane or the surface of a biomimetic object and therefore Y-junction formation is limited to the space close to the enzyme covered surface.

been employed previously to the actin network in the geometry of the lamellipodium [17]. However, this model has a viscoelastic character and stresses build up only transiently due to temporary cross-link formation and not due to static crosslinks formed close to the polymerizing interface of the network. The rigorous derivation of a macroscopic constitutive law of the network is therefore still lacking and is the subject of the present paper which takes up several ideas already outlined in [18].

One crucial observation is that actin forms a more or less periodic network on the microscopic scale, which is stable on the time scale of symmetry-breaking (i.e. several minutes). The size of each elementary cell, e.g. the distance between two links in the actin network (\sim several tens nm), is small compared to the total size of the structure ($\sim 1 \mu\text{m}$), which introduces a small parameter η into the problem and allows for the upscaling of the microscopic mechanical model to a continuous medium by discrete homogenization methods [19, 20, 21].

In this paper we apply the discrete homogenization method to a simple 2D network structure which has been “grown” from a circle. While we keep the network structure and the microscopic mechanical model simple, we retain crucial biological features. In the **Theory** section we will define the network topology along with the microscopic mechanical properties and derive a set of continuous equilibrium equations. In the **Results** section we will solve these equations for the axisymmetric equilibrium state and identify the conditions under which linearly stable solutions exist. Finally, in the **Conclusions** section we will give some perspectives for this homogenization approach in modeling actin networks.

2. Theory

In this section we derive the continuous equilibrium equations governing the homogenized network in an abstract Lagrangian coordinate frame. We start out with the discrete formulation of the network structure then upscale this description to a continuous medium. In a second step we introduce a free energy for the continuous medium and derive the equations of equilibrium using the first variation of the free energy. For completeness we outline in **Appendix A** and **Appendix B** the relation between the equilibrium description based on the stress vectors in the abstract Lagrangian frame as it is introduced in this **Theory** section and the classical Cauchy stress tensor.

2.1. Description of the discrete network

We consider a planar network around a solid circle of radius R_0 . The network consists of stiff elastic filaments linked at their ends by nodes. Its topology is shown in Fig. 2 on the left. The bars are attached to the cylinder surface at N_t sites evenly located at a distance $p = \eta R_0$, i.e. at an angular distance $\eta = 2\pi/N_t$. The network is made of N_n layers of bars in the radial direction. As the network was formed by polymerization of actin monomers at the surface of the cylinder, each radial layer contains the same number of nodes N_t . Each node can be identified by two integers $(\nu^1, \nu^2) \in \{0, \dots, N_n - 1\} \times \{0, \dots, N_t - 1\}$ as shown in Fig. 2 on the left. It is assumed that N_t and N_n are very large and of the same order. Consequently, $\eta = 2\pi/N_t$ is assumed to be very small and the parameter $\alpha = \eta N_n$ is of order 1 with respect to η .

$$(\mu^1, \mu^2) \Leftrightarrow (\lambda^1, \lambda^2)$$

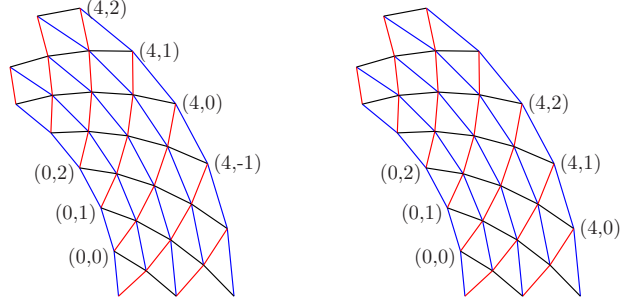


Figure 2: [Color online] Sketch of a small part of the filament network with some examples for the node numbering before (left) and after (right) the transformation of variables $(\mu^1, \mu^2) \rightarrow (\lambda^1, \lambda^2)$ as introduced in Eqs. (6) and (7). The “curves” along which $\mu^1 = \text{const.}$ and $\mu^2 = \text{const.}$ are shown in blue and red, respectively.

The elementary cell of such a network consists of one node and three bars $b = 1, 2, 3$ and is shown in Fig. 3. Orientation and length of each bar is described by the vector \vec{B}^b . The tension in the bars is described by a linear law

$$N^b = k^b \frac{l^b - l_m^b}{l_m^b} \quad (1)$$

with $l^b = \|\vec{B}^b\|$. k^b is a spring constant and l_m^b is the length of the bar b at rest. Here we will only consider the situation $k^1 = k^3$ and $l_m^1 = l_m^3$. At this stage the choice of a linear law is somewhat arbitrary and constitutes the simplest possible choice. It is consistent with basic principles in mechanics, such as material frame indifference. However, the homogenization procedure is valid for any microscopic law.

So far we have only considered forces associated with the lengths of the filaments and have not included the fact, that we are only interested in networks which keep a certain topology, e.g. the elementary cell has a finite area $\|\vec{B}^1 \wedge \vec{B}^3\| > 0$. To avoid this type of transition, i.e. a collapse of the network into zero area and a complete alignment of the vectors \vec{B}^b we add the following interaction moment between filaments 1 and 3

$$\vec{M}^{13} = M^{13} \vec{B}^1 \wedge \vec{B}^3 \quad (2)$$

with

$$M^{13} = \kappa \frac{(l^1 l^3)^2 (\vec{B}^1 \cdot \vec{B}^3)}{\left[(l^1 l^3)^2 - (\vec{B}^1 \cdot \vec{B}^3)^2 \right]^2} \quad (3)$$

where κ is a constant and denotes the interaction strength. As will be seen later in the derivation of the equilibrium equations in section 2.3, expressions (2) and (3) arise naturally from the first variation of the free energy which contains a potential which diverges for the complete alignment of \vec{B}^1 and \vec{B}^3 .

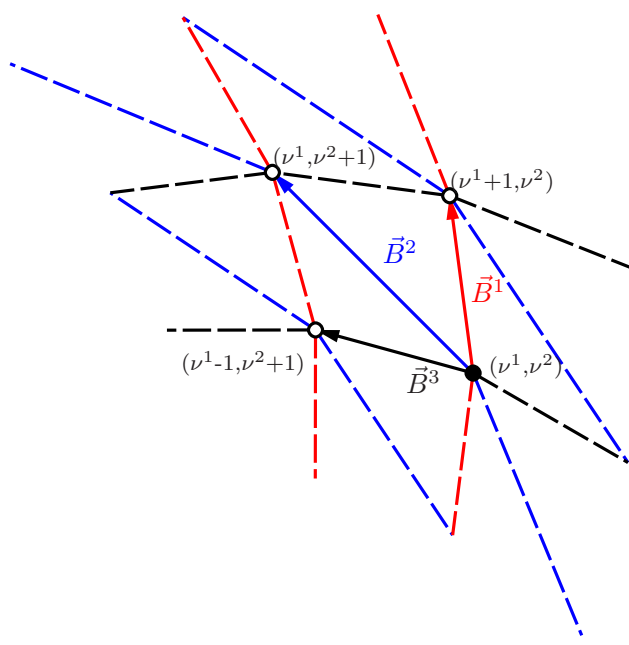


Figure 3: [Color online] Sketch of an elementary cell, showing the node numbering (ν^1, ν^2) and the elementary bar vectors \vec{B}^b (solid arrows). All other bars are shown as dashed lines. The “curves” along which $\nu^1=\text{const.}$ and $\nu^2=\text{const.}$ are shown in blue and red, respectively.

2.2. Homogenization

The upscaling of the network to a continuous medium consists in determining the equivalent stresses from the bar tensions, the equations of equilibrium (or motion) satisfied by these stresses and an equivalent constitutive equation ensuing from the properties of the bars. This can be carried out by using an asymptotic expansion (for an introduction see [22, 23, 20]). Here, as the network structure is simple, a more heuristic presentation can be used. The basic idea of the homogenization process is, that for most of the network motions, the positions of its nodes (ν^1, ν^2) can be approximated by a continuous deformation function $\vec{\psi}(\mu^1, \mu^2)$ such that the position of the node (ν^1, ν^2) is $\vec{\psi}(\mu^{1\eta}, \mu^{2\eta})$ with $\mu^{i\eta} = \eta\nu^i$ and $(\mu^{1\eta}, \mu^{2\eta}) \in \{0, \eta, \dots, \alpha - \eta\} \times \{0, \eta, \dots, 2\pi - \eta\}$. The discrete Lagrangian variables $(\mu^{1\eta}, \mu^{2\eta})$ become then the set of Lagrangian (curvilinear) coordinates $(\mu^1, \mu^2) \in \omega$ of the equivalent continuous medium with $\omega =]0, \alpha[\times]0, 2\pi[$.

In this homogenized network the filament vectors \vec{B}^b can now be expressed using a simple Taylor expansion up to $\mathcal{O}(\eta)$

$$\begin{aligned}\vec{B}^1 &= \eta \partial_{\mu^1} \vec{\psi} \\ \vec{B}^2 &= \eta \partial_{\mu^2} \vec{\psi}\end{aligned}\tag{4}$$

$$\vec{B}^3 = \eta \left(-\partial_{\mu^1} \vec{\psi} + \partial_{\mu^2} \vec{\psi} \right)\tag{5}$$

where $\partial_{\mu^i} = \frac{\partial}{\partial \mu^i}$. Since they are associated with a quite simple numbering system for the nodes, the variables μ^1 and μ^2 arise naturally as Lagrangian variables of the equivalent continuous medium through the homogenization process. However, they are not the most convenient variables to study axisymmetric equilibrium configurations. Therefore we have introduced the variables λ^1 and λ^2 defined by

$$\lambda^1 = \mu^1 \text{ and } \lambda^2 = \frac{\mu^1}{2} + \mu^2\tag{6}$$

and which correspond to the radial and angular position of the node in the network [see Fig. 2 to the right]. Setting

$$\vec{\varphi}(\lambda^1, \lambda^2) = \vec{\psi} \left(\lambda^1, -\frac{\lambda^1}{2} + \lambda^2 \right)\tag{7}$$

one finds

$$\begin{aligned}\vec{B}^1 &= \eta \left(\vec{h}_1 + \frac{1}{2} \vec{h}_2 \right) \\ \vec{B}^2 &= \eta \vec{h}_2 \\ \vec{B}^3 &= \eta \left(-\vec{h}_1 + \frac{1}{2} \vec{h}_2 \right)\end{aligned}\tag{8}$$

with $\vec{h}_1 = \partial_{\lambda^1} \vec{\varphi}$ and $\vec{h}_2 = \partial_{\lambda^2} \vec{\varphi}$ where $\partial_{\lambda^i} = \frac{\partial}{\partial \lambda^i}$. In the following we will employ the simplified notation $\partial_i = \partial_{\lambda^i}$.

2.3. Equations of equilibrium

The equations of equilibrium can be obtained directly by following the homogenization procedure up to first order in η detailed in [21]. However, here we have chosen a simpler approach using only the filament vectors \vec{B}^b obtained by homogenization and by defining a free elastic energy F of the network corresponding to the constitutive functions N^b and the moment \vec{M}^{13} defined in (1) and (2). This free energy F can be expressed as the functional

$$F[\vec{\varphi}] = \frac{1}{\eta^2} \int_{\omega} \left[\sum_{b=1}^3 \frac{k^b}{2l_m^b} (l^b - l_m^b)^2 + \frac{\kappa}{2} \frac{(\vec{B}^1 \cdot \vec{B}^3)^2}{(l^1 l^3)^2 - (\vec{B}^1 \cdot \vec{B}^3)^2} \right] d\lambda^1 d\lambda^2 \quad (9)$$

where $l^b = \|\vec{B}^b\|$. The first sum in (9) denotes the free energy associated with the compression and elongation of the filaments. The second term is associated with the interaction between the filaments 1 and 3 and serves as a ‘‘hard core’’ potential, which prevents the collapse of the networks, i.e. it prevents the complete alignment of the filaments 1 and 3.

The first variation of F with respect to the deformation function $\vec{\varphi}$ reads

$$\begin{aligned} \delta F &= \frac{1}{\eta^2} \int_{\omega} d\lambda^1 d\lambda^2 \left\{ \sum_{b=1}^3 N^b \frac{\vec{B}^b}{l^b} \cdot \delta \vec{B}^b + \right. \\ &\quad \left. \left(\vec{M}^{13} \wedge \frac{\vec{B}^1}{(l^1)^2} \right) \cdot \delta \vec{B}^1 - \left(\vec{M}^{13} \wedge \frac{\vec{B}^3}{(l^3)^2} \right) \cdot \delta \vec{B}^3 \right\} \\ &= \frac{1}{\eta} \int_{\omega} d\lambda^1 d\lambda^2 \left(\vec{S}^1 \cdot \delta \vec{h}_1 + \vec{S}^2 \cdot \delta \vec{h}_2 \right), \end{aligned} \quad (10)$$

where the stress vectors \vec{S}^1 and \vec{S}^2 are given by

$$\vec{S}^1 = \frac{N^1}{l^1} \vec{B}^1 - \frac{N^3}{l^3} \vec{B}^3 + \vec{M}^{13} \wedge \left[\frac{\vec{B}^1}{(l^1)^2} + \frac{\vec{B}^3}{(l^3)^2} \right] \quad (11)$$

$$\vec{S}^2 = \frac{N^1}{2l^1} \vec{B}^1 + \frac{N^2}{l^2} \vec{B}^2 + \frac{N^3}{2l^3} \vec{B}^3 + \frac{1}{2} \vec{M}^{13} \wedge \left[\frac{\vec{B}^1}{(l^1)^2} - \frac{\vec{B}^3}{(l^3)^2} \right] \quad (12)$$

Integrating Eq. (10) by parts and taking into account the periodicity in λ^2 (i.e. the integrals along the boundaries of the network with $\lambda^2 = 0$ and $\lambda^2 = 2\pi$ cancel each other out) one finds

$$\begin{aligned} \delta F &= -\frac{1}{\eta} \int_{\omega} \left(\partial_1 \vec{S}^1 + \partial_2 \vec{S}^2 \right) \cdot \delta \vec{\varphi} d\lambda^1 d\lambda^2 \\ &\quad + \frac{1}{\eta} \int_0^{2\pi} \vec{S}^1(\alpha, \lambda^2) \cdot \delta \vec{\varphi} d\lambda^2 - \frac{1}{\eta} \int_0^{2\pi} \vec{S}^1(0, \lambda^2) \cdot \delta \vec{\varphi} d\lambda^2 \end{aligned} \quad (13)$$

The last two integrals over the boundary at $\lambda^1 = 0$ and $\lambda^1 = \alpha$ in Eq. (13) evaluate to zero since $\vec{\varphi}$ is fixed at the internal boundary, i.e. $\delta \vec{\varphi} = 0$ for $\lambda^1 = 0$, and there are

no normal forces acting on the external surface, i.e. $\boldsymbol{\sigma} n = \vec{S}^1 / \|\vec{h}^2\| = 0$ for $\lambda^1 = \alpha$. Here $\boldsymbol{\sigma}$ denotes the Cauchy stress tensor (see **Appendix B**) and \vec{n} is the unit outward surface normal vector in the deformed configuration.

The mechanical equilibrium in the absence of volumic forces is therefore given by

$$0 = \partial_1 \vec{S}^1 + \partial_2 \vec{S}^2 \quad (14)$$

with the boundary conditions as mentioned before

$$\begin{aligned} \forall \lambda^1 &\in]0, \alpha[, \quad \vec{\varphi}(\lambda^1, 0) = \vec{\varphi}(\lambda^1, 2\pi) \\ \forall \lambda^2 &\in]0, 2\pi[, \quad \vec{\varphi}(0, \lambda^2) = R_0 \vec{e}_r(\lambda^2) \\ \forall \lambda^2 &\in]0, 2\pi[, \quad \vec{S}^1(\alpha, \lambda^2) = 0 \end{aligned} \quad (15)$$

where $\vec{e}_r = \cos \lambda^2 \vec{e}_1 + \sin \lambda^2 \vec{e}_2$ denotes the unit vector in the radial direction in the orthonormal coordinate basis $\{\vec{e}_1, \vec{e}_2\}$. For a later use we introduce here also the tangential unit vector as $\vec{e}_\theta = -\sin \lambda^2 \vec{e}_1 + \cos \lambda^2 \vec{e}_2$.

3. Results

3.1. Axisymmetric state

In the following we will use the simplified notation $\varphi'_r = \partial_1 \varphi_r$. Eq. (14) with the boundary conditions (15) was analyzed for axisymmetric solutions of the type $\vec{\varphi} = \varphi_r(\lambda^1) \vec{e}_r$. The stress vectors (11) and (12) can then be simplified to

$$\vec{S}^1 = \eta \left\{ 2 \frac{N^1}{l^1} \varphi'_r - M^{13} \varphi_r^2 \varphi'_r \right\} \vec{e}_r \quad (16)$$

$$\vec{S}^2 = \eta \left\{ \frac{N^1}{2l^1} \varphi_r + \frac{N^2}{l^2} \varphi_r + M^{13} \varphi_r \varphi_r'^2 \right\} \vec{e}_\theta \quad (17)$$

The equilibrium equation (14) becomes

$$0 = \partial_1 \left(2 \frac{N^1}{l^1} \varphi'_r - M^{13} \varphi_r^2 \varphi'_r \right) - \left(\frac{1}{2} \frac{N^1}{l^1} \varphi_r + \frac{N^2}{l^2} \varphi_r + M^{13} \varphi_r \varphi_r'^2 \right) \quad (18)$$

with the boundary conditions

$$\begin{aligned} \varphi_r(0) &= R_0 \\ 0 &= \left[2 \frac{N^1}{l^1} \varphi'_r - M^{13} \varphi_r^2 \varphi'_r \right]_{\lambda^1 = \alpha} \end{aligned} \quad (19)$$

Eq. (18) was solved using continuation techniques [24] and the solutions were characterized using the equilibrium network thickness $H = \varphi_r(\alpha) - R_0$ and the associated free energy (9).

At this stage we point out that the unknown function $\varphi_r(\lambda^1)$ needs only to be piecewise continuously differentiable. It can have ‘‘corner points’’, i.e. discontinuities in the first order derivative. The presence of such discontinuous solutions can

be inferred from the fact that $\partial^2 f / \partial \varphi_r'^2$ vanishes for a finite value φ_r' at the “corner point” $(\lambda_d^1, \varphi_{rd})$. For every continuously differentiable segment of an extremal solution Eq. (18) holds supplemented by the following boundary conditions at the “free corner points” [25]

$$[\partial f / \partial \varphi_r']_{\lambda^1 = \lambda_d^1 - 0} = [\partial f / \partial \varphi_r']_{\lambda^1 = \lambda_d^1 + 0} \quad (20)$$

$$[f - \varphi_r' \partial f / \partial \varphi_r']_{\lambda^1 = \lambda_d^1 - 0} = [f - \varphi_r' \partial f / \partial \varphi_r']_{\lambda^1 = \lambda_d^1 + 0} \quad (21)$$

The first condition (20) is equivalent to the physical boundary condition, that the normal stresses match at the “cornerpoint”. The second condition (21) minimizes the energy with respect to the position of the “corner point”.

First one might consider the special case $k^2 = \kappa = 0$. As it is easy to see, $N^1 = 0$ solves Eqs. (18) and (19). Under the condition that $l_m^1 \geq p/2$ (recall that p denotes the distance at which the nodes are attached at the cylinder surface) one therefore finds the equilibrium solution

$$\frac{\varphi_r}{R_0} = \frac{2l_m^1}{p} \sin \left[\frac{\lambda^1}{2} + \arcsin \left(\frac{p}{2l_m^1} \right) \right]. \quad (22)$$

At the radial layer number $\lambda^1 = \lambda_c^1 = \pi - 2 \arcsin \left(\frac{p}{2l_m^1} \right)$ one finds $\varphi_r' = 0$ and $\varphi_r / R_0 = 2l_m^1 / p$. At this point the network collapses to zero volume and the filaments \vec{B}^1 , \vec{B}^2 and \vec{B}^3 are oriented in parallel. The addition of further network layers will either lead to a back-folding of the gel into itself (in this case solution (22) holds), or the network layer will rest in this collapsed state, i.e. $\varphi_r / R_0 = 2l_m^1 / p$ for $\lambda^1 > \lambda_c^1$. In this case λ_c^1 constitutes a “corner point”, where Eqs. (20) and (21) hold.

The back-folding behavior is excluded in a physical situation since it requires the remodeling of the network structure and in the following we will not consider these special cases. The network collapse is unphysical as well since it implies a zero volume of the network layers.

Now we will consider the more physical case $k^2 > 0$. Fig. 4 shows the dependence of the equilibrium network thickness H and the associated energy depending on the number of radial network layers α for the case $k = k^2 / k^1 = 1$ and $l_m^1 = l_m^2 = p$, i.e. all filaments are identical and type 2 filaments are inserted at the internal interface at their equilibrium length. First, increasing the ratio of the elastic constant k^2 / k^1 decreases the network thickness H for a constant number of radial network layers α . Second, the continuously differentiable solution branches with $\varphi_r' > 0$ cease to exist beyond a critical value α_c . Instead solutions appear which have one or more discontinuities in φ_r' and which contain solution segments with $\varphi_r' < 0$ (not shown).

To exclude the back-folding behavior we have added an additional term in the free energy related to the interaction between \vec{B}^1 and \vec{B}^3 and which prevents the alignment of \vec{B}^1 and \vec{B}^3 . Fig. 4 shows exemplary the network thickness and free energy for a small value of κ / k^1 . Solutions exist even for very large networks and the solution behavior for small networks is similar to the behavior with $\kappa = 0$.

Fig. 5 shows exemplary solutions for Eq. (18) for small, intermediate and large networks. For small and intermediate networks, the filament lengths and stresses increase almost linearly with λ^1 , whereas for large networks the behavior is strongly nonlinear.

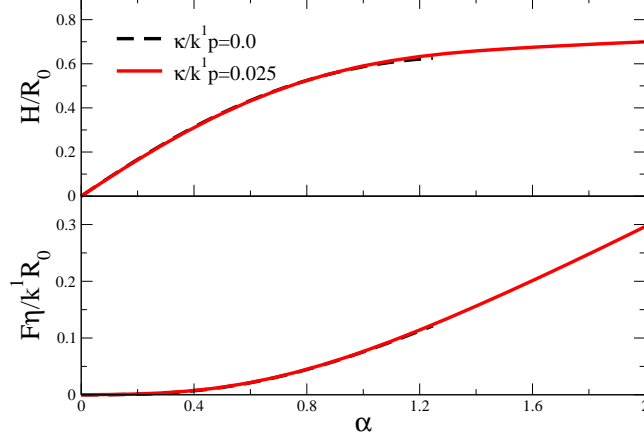


Figure 4: [Color online] (a) Equilibrium thickness of the network H and (b) the associated energy depending on the number of radial network layers α for $\kappa = 0$ and $\kappa/k^1 p = 0.025$ as indicated in the legend. Remaining parameters are $k_2/k_1 = 1$ and $l_m^1 = l_m^2 = p$.

The network is always under radial compression, whereas it is under tangential compression close to the surface of the obstacle and under tangential extension at the outer surface of the network.

3.2. Linear stability

To study the (mechanical) linear stability of the axisymmetric state we have evaluated the sign of the second variation of F with respect to $\vec{\varphi}$ at the prestress axisymmetric state $\varphi_r \vec{e}_r$

$$\delta^2 F = \int_{\omega} \delta \vec{h}_i \frac{\partial^2 f}{\partial \vec{h}_i \partial \vec{h}_j} \delta \vec{h}_j d\lambda^1 d\lambda^2 \quad (23)$$

with the boundary conditions

$$\begin{aligned} \forall \lambda^1 &\in]0, \alpha[, \delta \vec{\varphi}(\lambda^1, 0) = \delta \vec{\varphi}(\lambda^1, 2\pi) \\ \forall \lambda^2 &\in]0, 2\pi[, \delta \vec{\varphi}(0, \lambda^2) = 0 \end{aligned} \quad (24)$$

Details of the stability analysis can be found in **Appendix C**. Briefly, we have used a Fourier mode decomposition of $\delta \vec{\varphi}$ and a direct integration in λ^2 and finite elements for a numerical integration in the λ^1 .

Fig. 6 shows the linear stability of $\varphi_r(\lambda^1)$ depending on the elastic ratio k^2/k^1 and α . The linear stability of the axisymmetric state depends on the number of radial network layers superimposed over each other, whereby thin networks are stable and thick networks are unstable. Furthermore, networks with higher tangential stresses (large k^2/k^1) destabilize at smaller α . The instability occurs independently of the transversal wavenumber m and is accompanied by the appearance of a region adjacent to the inner interface where $\partial^2 f / \partial h_{1\theta}^2 < 0$. The appearance of the instability is probably due to the fact, that as the network thickness increases the compressive load acting on type 1 and

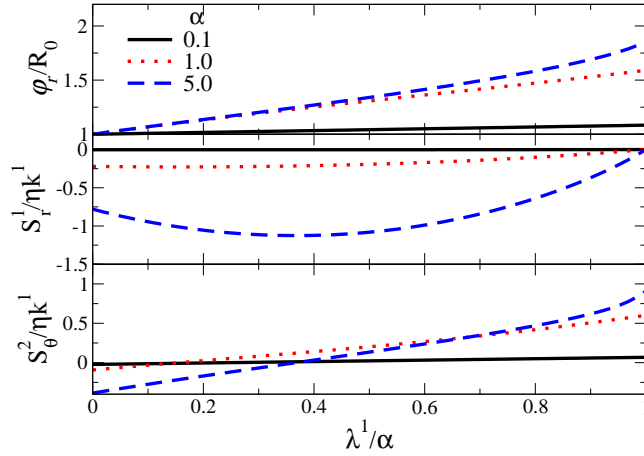


Figure 5: [Color online] Solutions of Eq. 18 for different network thicknesses α as indicated in the legend. Shown is (a) the radial node position, (b) the radial stress, and (c) the tangential stress distribution. Remaining parameters are $k^2/k^1 = 1$, $\kappa/k^1 p = 0.025$, $l_m^1 = l_m^2 = p$.

type 3 filaments in the innermost network layers increases. The elastic stress is released by rotating consecutive network layers against each other. Since the model does not contain any force opposed to a change in orientation of consecutive filaments of type 1 and 3, which introduce an additional length scale related to a “persistence length” of consecutive filaments of the same type, a catastrophic growth of the instability at infinitely small scales occurs (data not shown).

4. Conclusions

We have introduced a two-dimensional homogenization model to describe the mechanics of stiff elastic filament networks assembled on a cylindrical surface resembling Arp2/3 cross-linked actin networks as they occur in living cells. Our approach allows us to realistically model macroscopic deformations and stresses due to network growth by using only assumptions about the microscopic network properties. The main purpose of the model is to introduce a minimal set of mechanical ingredients as a basis for the more advanced problem of the time-dependent evolution of the network interfaces due to polymerization/depolymerization at the interface with a possible symmetry-breaking and subsequent motion.

The approach is novel in the field of actin driven motion, inasmuch as it allows to calculate equilibrium stresses and the position of the interface between the network and the surrounding solution without any ad hoc assumptions [14] or restrictions to infinitesimal deformations [16]. Furthermore it will allow a rigorous calculation of the equilibrium state for networks with perturbed interfaces, resulting from spontaneous variations in the polymerization or depolymerization speed at the network interfaces as outlined in [18]. However, in this study we have limited ourselves to fixed interfaces

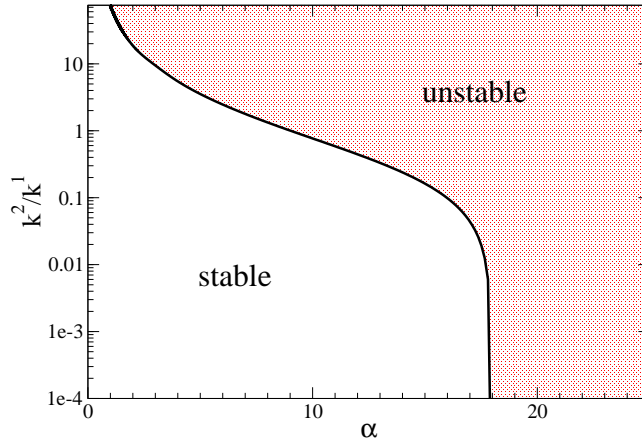


Figure 6: Linear stability of continuously differentiable axisymmetric solutions depending on the parameters k^2/k^1 and α . Above (below) the solid line axisymmetric solutions are linearly unstable (stable). Remaining parameters are $l_m^1 = l_m^2 = p$ and $\kappa/k^1 p = 0.025$.

(in the Lagrangian frame) and studied the existence and linear stability of physical and biological relevant axisymmetric equilibrium states.

We find that in a triangular network where only changes in the length of the edges contribute to the free energy the existence of sensible solutions is limited by the number of radial network layers α superimposed over each other. As one increases α beyond a critical number the network starts to fold back into the negative radial direction, since the extension of the microscopic filaments in the tangential direction is unfavorable as one moves away from the cylinder surface. The inclusion of an additional term in the free energy related to the interaction between two selected filaments prevented this back-folding.

Furthermore, the linear stability of the axisymmetric solution depends on the microscopic elastic properties. In general, thin networks are stable and thick networks are unstable, whereby a higher elastic constant for filaments oriented in the tangential direction favors the occurrence of the instability for thinner networks. The instability is independent of the transversal wavenumber of the harmonic perturbations. A closer inspection of the instability reveals that it occurs first at the cylinder surface and is reminiscent of a buckling instability of type 1 and 3 filament, i.e. a counterrotation of consecutive radial network layers. However, there is no mechanism in this simple model to stabilize this instability. A more advanced approach would have to include a more detailed microscopic mechanical model with nonlocal contributions (i.e. in the spirit of second gradient model), which is beyond the scope of this paper and will be the subject of further investigation.

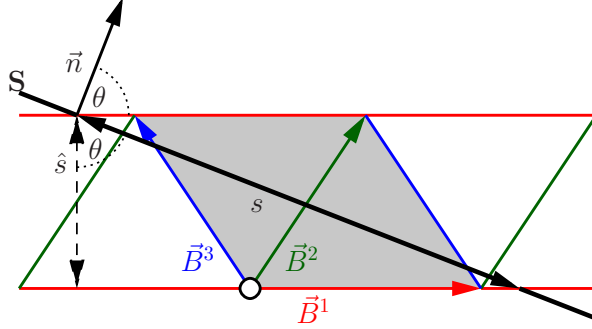


Figure A.7: A facet S with the unit normal \vec{n} and the segment length s is placed in the network. The elementary cell with the basis vectors \vec{B}^b and the height \hat{s} is shown in gray.

Appendix A. Derivation of the Cauchy stress tensor in the network

The first to define a stress tensor in a discrete medium in the Lagrangian frame were Cauchy and Poisson whose derivation can be found in [23, 22]. We present here the basic ideas in two dimensions to facilitate the comprehension of the **Theory** section.

For the derivation of the stress one considers a periodic structure of nodes and their connections. Forces act only along the directions of the node connections. The periodic structure is divided into elementary cells which are numbered by (ν^1, ν^2) . The connections are identified by the triplet (b, ν^1, ν^2) , where b identifies the connection within the elementary cell.

The stress tensor is defined over a force \vec{R} acting on an arbitrary facet S with unit normal \vec{n} placed in the periodic medium as shown in Fig. A.7. The force \vec{R} is obtained by summing up the forces acting along the node connections which are cut by the facet. Thereby one assumes that the length S of the facet is sufficiently small that the forces exerted by identical connections are constant over the facet. Therefore the force \vec{R} is given by

$$\vec{R} = \sum_b m^b \text{sgn}(\vec{B}^b \cdot \vec{n}) N^b \frac{\vec{B}^b}{\|\vec{B}^b\|}. \quad (\text{A.1})$$

Here N^b and m^b denote the tension and number of node connections of type b . The term $\text{sgn}(\vec{B}^b \cdot \vec{n})$ accounts for the orientation of the connections. There are different ways to determine m^b , we give here only the result derived in detail in [22]. The basic idea is, that the facet S is cut by the vectors of one type b into segments s and therefore $m^b = S/s$. As can be seen in Fig. A.7 for the example of the type 1 filament, the height of the elementary cell is $\hat{s} = s|\vec{B}^1 \cdot \vec{n}|/\|\vec{B}^1\|$ and consequently its area is given by $A_c = \hat{s}\|\vec{B}^1\|$. Therefore the number of links of type b cut by the facet S can be expressed as

$$m^b = \frac{S|\vec{B}^b \cdot \vec{n}|}{A_c} \quad (\text{A.2})$$

Using expression (A.2) with Eq. (A.1) one obtains

$$\vec{R} = \frac{1}{A_c} \sum_b N^b \frac{\vec{B}^b}{\|\vec{B}^b\|} (\vec{B}^b \cdot \vec{n}) S. \quad (\text{A.3})$$

After some rearrangements and using the identity

$$\vec{R} = \sigma \vec{n} S \quad (\text{A.4})$$

one finds

$$\sigma = \frac{1}{A_c} \sum_b N^b \frac{\vec{B}^b \otimes \vec{B}^b}{\|\vec{B}^b\|} \quad (\text{A.5})$$

Appendix B. Relation between the stress vectors \vec{S}^i and the Cauchy stress tensor σ

In the present section we demonstrate the relation between the classical equilibrium equation known from continuum mechanics using the Cauchy stress tensor σ in the deformed configuration and the equilibrium formulation we have used throughout this paper defined on the Lagrangian reference configuration. Note, that we will use the Einstein notation, i.e. summation over repeated indices, and that we will use the abbreviation $\partial_i = \partial_{\lambda^i}$ which denotes a partial derivation with respect to the coordinate λ^i in the Lagrangian reference configuration.

We start out by introducing some equalities. Let $\vec{\varphi}$ be the deformation mapping of the network with respect to its Lagrangian configuration ω and let $\vec{x} = \vec{\varphi}(\lambda^1, \lambda^2)$ be the position in the deformed configuration $\omega_\varphi = \vec{\varphi}(\omega)$ of the network point (λ^1, λ^2) of the Lagrangian reference configuration. Let $d\vec{x}$ be the difference of positions of two neighbouring points (λ^1, λ^2) and $(\lambda^1 + d\lambda^1, \lambda^2 + d\lambda^2)$, then

$$d\vec{x} = \vec{h}_i d\lambda^i \quad (\text{B.1})$$

where $\vec{h}_i = \partial_i \vec{\varphi}$. Consequently one finds

$$d\lambda^i = \vec{h}^i \cdot d\vec{x} \quad (\text{B.2})$$

with the property

$$\vec{h}_i \cdot \vec{h}^j = \delta_i^j \quad (\text{B.3})$$

Let now \vec{v} be a virtual velocity field which, due to the one to one mapping $\vec{\varphi}$ from ω to ω_φ , can be considered either as a function of λ^1, λ^2 or as a function of \vec{x} . \vec{v} is assumed to be differentiable and let $\nabla \vec{v}$ be its differential with respect to \vec{x} and $\partial_i \vec{v}$ be its partial derivative with respect to λ^i , then

$$d\vec{v} = \nabla \vec{v} d\vec{x} \quad (\text{B.4})$$

$$d\vec{v} = \partial_i \vec{v} d\lambda^i \quad (\text{B.5})$$

Now, the use of equations (B.1) and (B.2) yields

$$\nabla \vec{v} = \partial_i \vec{v} \otimes \vec{h}^i \quad (\text{B.6})$$

$$\partial_i \vec{v} = \nabla \vec{v} \vec{h}_i \quad (\text{B.7})$$

In the absence of body forces the virtual power formulation of the equilibrium equation (14) reads

$$\int_{\omega} \vec{S}^i \cdot \partial_i \vec{v} d\lambda^1 d\lambda^2 = 0 \quad (\text{B.8})$$

where the virtual velocity field \vec{v} vanishes on the boundaries $\lambda^1 = 0$ and $\lambda^1 = \alpha$ of ω and is 2π periodic with respect to λ^2 .

The change of variables $(\lambda^1, \lambda^2) \leftrightarrow \vec{x} = \varphi(\lambda^1, \lambda^2)$ in the intergral of the previous equation yields

$$\int_{\omega_\varphi} \vec{S}^i \cdot (\nabla \vec{v} \vec{h}_i) \frac{1}{h} ds = 0 \quad (\text{B.9})$$

where $ds = h d\lambda^1 d\lambda^2$ denotes the area element of the body in the deformed configuration with $h = \|\vec{h}_1 \wedge \vec{h}_2\|$. The previous equation also reads

$$\int_{\omega_\varphi} \frac{1}{h} \left(\vec{S}^i \otimes \vec{h}^i \right) : \nabla \vec{v} ds = 0 \quad (\text{B.10})$$

where $\mathbf{A} : \mathbf{B}$ denotes the usual twice contracted product between the second order tensors \mathbf{A} and \mathbf{B} .

Comparing with the classical virtual power formulation of the equilibrium in the Eulerian variable \vec{x} which reads

$$\int_{\omega_\varphi} \boldsymbol{\sigma} : \nabla \vec{v} ds = 0 \quad (\text{B.11})$$

we can see that the expression of the Cauchy stres tensor $\boldsymbol{\sigma}$ in terms of the \vec{S}^i 's reads

$$\boldsymbol{\sigma} = \frac{1}{h} \vec{S}^i \otimes \vec{h}_i \quad (\text{B.12})$$

Conversely, the use of definition (B.3) of the contravariant base (\vec{h}^1, \vec{h}^2) in the equation (B.12) yields the expressions of the vectors \vec{S}^1 and \vec{S}^2 in terms of $\boldsymbol{\sigma}$ which reads

$$\vec{S}^i = h \boldsymbol{\sigma} \vec{h}^i \quad (\text{B.13})$$

Appendix C. Linear stability analysis

Since the boundary conditions are periodic in λ^2 one can decompose $\delta\vec{\varphi} = \delta\varphi_r\vec{e}_r + \delta\varphi_\theta\vec{e}_\theta$ into a Fourier series

$$\begin{aligned}\delta\varphi_r &= \sum_{m=0}^{\infty} [\delta\varphi_{rc}^m(\lambda^1) \cos(m\lambda^2) + \delta\varphi_{rs}^m(\lambda^1) \sin(m\lambda^2)] \\ \delta\varphi_\theta &= \sum_{m=0}^{\infty} [\delta\varphi_{\theta c}^m(\lambda^1) \cos(m\lambda^2) + \delta\varphi_{\theta s}^m(\lambda^1) \sin(m\lambda^2)]\end{aligned}\tag{C.1}$$

where m denotes the wavenumber and $\delta\varphi_{rc}^m, \delta\varphi_{rs}^m, \delta\varphi_{\theta c}^m, \delta\varphi_{\theta s}^m$ denote perturbation amplitudes which depend only on λ^1 . Using ansatz (C.1) one can perform the integration of (23) in λ^2 directly whereby different wavenumbers m decouple. One finds then

$$\delta^2 F = \pi \sum_{m=0}^{\infty} \int_0^\alpha (\delta^2 f_1^m + \delta^2 f_2^m) d\lambda^1\tag{C.2}$$

where $\delta^2 f_{1,2}^m$ takes the form

$$\begin{aligned}\delta^2 f_{1,2}^m &= A(a')^2 + B(b')^2 + 2C(a'a + ma'b) - \\ &\quad 2D(b'b + ma'b) + E(ma + b)^2 + F(a + mb)^2\end{aligned}\tag{C.3}$$

with $(a, b) = (\delta\varphi_{rc}^m, \delta\varphi_{\theta s}^m)$ and $(a, b) = (-\delta\varphi_{rs}^m, \delta\varphi_{\theta c}^m)$ for $\delta^2 f_1^m$ and $\delta^2 f_2^m$, respectively. The factors A, \dots, F are evaluated at the axisymmetric solution $\vec{\varphi} = \varphi_r\vec{e}_r$ and are given by

$$\begin{aligned}A &= \frac{\partial^2 f}{\partial h_{1r}^2} = 2\frac{N^1}{l^1} + 2k^1 \frac{\varphi_r'^2}{(l^1)^3} + \kappa \frac{3\varphi_r^4/16 - \varphi_r'^4}{\varphi_r^2\varphi_r'^4} \\ B &= \frac{\partial^2 f}{\partial h_{1\theta}^2} = 2\frac{N^1}{l^1} + k^1 \frac{\varphi_r'^2}{2(l^1)^3} - 2\kappa \frac{\varphi_r^2/4 - \varphi_r'^2}{\varphi_r^2\varphi_r'^2} \\ C &= \frac{\partial^2 f}{\partial h_{1r}\partial h_{2\theta}} = k^1 \frac{\varphi_r\varphi_r'}{2(l^1)^3} - 2\kappa \frac{\varphi_r^4/16 + \varphi_r'^4}{\varphi_r^3\varphi_r'^3} \\ D &= \frac{\partial^2 f}{\partial h_{1\theta}\partial h_{2r}} = k^1 \frac{\varphi_r\varphi_r'}{2(l^1)^3} + \kappa \frac{(\varphi_r^2/4 - \varphi_r'^2)^2}{\varphi_r^3\varphi_r'^3} \\ E &= \frac{\partial^2 f}{\partial h_{2r}^2} = \frac{N^1}{2l^1} + \frac{N^2}{l^2} + k^1 \frac{\varphi_r'^2}{2(l^1)^3} + \kappa \frac{\varphi_r^2/4 - \varphi_r'^2}{2\varphi_r^2\varphi_r'^2} \\ F &= \frac{\partial^2 f}{\partial h_{2\theta}^2} = \frac{N^1}{2l^1} + \frac{N^2}{l^2} + k^1 \frac{\varphi_r'^2}{8(l^1)^3} + k^2 \frac{\varphi_r'^2}{(l^2)^3} + \\ &\quad \kappa \frac{\varphi_r^4/16 + 3\varphi_r'^4}{\varphi_r^4\varphi_r'^2}\end{aligned}$$

The integral (C.2) was calculated numerically by using finite elements, whereby the functions $\delta\varphi_{rs}^m$, $\delta\varphi_{rc}^m$, $\delta\varphi_{\theta s}^m$, and $\delta\varphi_{\theta c}^m$ were approximated by P_1 -elements and the functions A, \dots, F were approximated by P_0 elements. This results in the quadratic form

$$\delta^2 F = \sum_{m=0}^{\infty} \{(\hat{\varphi}_{rc}^m, \hat{\varphi}_{\theta s}^m) \mathbf{Q}^m (\hat{\varphi}_{rc}^m, \hat{\varphi}_{\theta s}^m)^T + (-\hat{\varphi}_{rs}^m, \hat{\varphi}_{\theta c}^m) \mathbf{Q}^m (-\hat{\varphi}_{rs}^m, \hat{\varphi}_{\theta c}^m)^T\} \quad (\text{C.4})$$

where $\hat{\cdot}$ indicates a vector containing function values evaluated at the discretization points λ_i^1 , ($i = 1, 2, \dots, n$) and \mathbf{Q}^m is a symmetric $2n \times 2n$ matrix.

For the axisymmetric state to be linearly stable $\delta^2 F > 0$, i.e. \mathbf{Q}^m needs to be a positive definite matrix. We have tested this condition for wavenumbers $m \leq 4$. But it turned out that an instability appears independently of m when the factor $B = \partial^2 f / \partial h_{1\theta}^2$ changes sign at $\lambda^1 = 0$. The corresponding phase diagram is shown in Fig. 6.

References

- [1] T. P. Loisel, R. Boujema, D. Pantaloni, M.-F. Carrier, Reconstitution of actin-based motility of listeria and shigella using pure proteins, *Nature* 401 (1999) 613–616.
- [2] J. Taunton, B. A. Rowning, M. L. Coughlin, M. Wu, R. T. MoOn, T. J. Mitchison, C. A. Larabell, Actin-dependent propulsion of endosomes and lysosomes by recruitment of n-wasp, *J. Cell Biol.* 148 (2000) 519–530.
- [3] D. Yarar, W. To, A. Abo, M. D. Welch, The Wiskott-Aldrich syndrome protein directs actin-based motility by stimulating actin nucleation with the Arp2/3 complex, *Curr. Biol.* 9 (1999) 555–558.
- [4] S. Cudmore, P. Cossart, G. Griffiths, M. Way, Actin-based motility of vaccinia virus, *Nature* 378 (1995) 636–638.
- [5] A. van Oudenaarden, J. A. Theriot, Cooperative symmetry-breaking by actin polymerization in a model for cell motility, *Nature Cell Biol.* 1 (1999) 493–499.
- [6] A. Upadhyaya, J. Chabot, A. Andreeva, A. Samadani, A. van Oudenaarden, Probing polymerization forces by using actin-propelled lipid vesicles, *Proc. Nat. Acad. Sci.* 100 (2003) 4521–4526.
- [7] H. Boukellal, O. Campás, J.-F. Joanny, P. J., C. Sykes, Soft listeria: Actin-based propulsion of liquid drops, *Phys. Rev. E* 69 (2004) 061906.
- [8] T. D. Pollard, L. Blanchoin, R. D. Mullins, Molecular mechanisms controlling actin filament dynamics in nonmuscle cells, *Ann. Rev. Biophys. Biomol. Struct.* 29 (2000) 545–576.
- [9] M. J. Footer, J. W. J. Kerssemakers, J. A. Theriot, M. Dogterom, Direct measurement of force generation by actin filament polymerization using an optical trap, *Proc. Natl. Acad. Sci. USA* 104 (2007) 2181–2186.

- [10] V. Noireaux, R. M. Golsteyn, E. Friederich, J. Prost, C. Antony, D. Louvard, C. Sykes, Growing an actin gel on spherical surfaces, *Biophys. J.* 78 (2000) 1643–1654.
- [11] J. van der Gucht, E. Paluch, J. Plastino, C. Sykes, Stress release drives symmetry breaking for actin-based movement, *PNAS* 102 (2005) 7847–7852.
- [12] V. Delatour, S. Shekhar, A.-C. Reyman, D. Didry, K. Hô Diêp Lê, G. Romet-Lemonne, E. Helfer, M.-F. Carlier, Actin-based propulsion of functionalized hard versus fluid spherical objects, *New J. Phys.* 10 (2008) 025001.
- [13] A. Mogilner, G. Oster, Force generation by actin polymerization ii: The elastic ratchet and tethered filaments, *Biophys. J.* 84 (2003) 1591–1605.
- [14] K. Sekimoto, J. Prost, F. Jülicher, H. Boukellal, A. Bernheim-Grosswasser, Role of tensile stress in actin gels and a symmetry-breaking instability, *Eur. Phys. J. E* 13 (2004) 247–259.
- [15] A. Lee, H. Y. Lee, M. Kardar, Symmetry-breaking motility, *Phys. Rev. Lett.* 95 (2005) 138101.
- [16] K. John, P. Peyla, K. Kassner, J. Prost, C. Misbah, Nonlinear study of symmetry-breaking in actin gels: Implications for cellular motility, *Phys. Rev. Lett.* 100 (2008) 068101.
- [17] D. Oelz, N. Schmeiser, V. Small, Modeling of the actin-cytoskeleton in symmetric lamellipodial fragments, *Cell Adh. Migr.* 2 (2008) 117–126.
- [18] K. John, D. Caillerie, P. Peyla, M. Ismail, A. Raoult, J. Prost, C. Misbah, *Cell mechanics. From single scale-based models to multiscale modeling*, CRC Press, Chapman & Hall, 2009, Ch. Actin based propulsion: Intriguing interplay between material properties and growth processes.
- [19] G. Moreau, D. Caillerie, Continuum modeling of lattice structures in large displacement applications to buckling analysis, *Comp. Struct.* 68 (1998) 181–189.
- [20] H. Tollenaere, D. Caillerie, Continuous modelling of lattice structures by homogenization, *Adv. Engin. Softw.* 29 (1998) 699–705.
- [21] D. Caillerie, A. Mourad, A. Raoult, Cell-to-muscle homogenization. Application to a constitutive law for the myocardium, *ESAIM: Math. Model. Num. Anal.* 37 (2003) 681–698.
- [22] D. Caillerie, B. Cambou, *Micromécanique des milieux granulaires*, Vol. 108, Hermès Sciences, 2001, Ch. Les techniques de changement d'échelles dans les matériaux granulaires.
- [23] A. E. H. Love, *A treatise of the mathematical theory of elasticity*, Dover, New York, 1944.

- [24] E. J. Doedel, A. R. Champneys, T. F. Fairgrieve, Y. A. Kuznetsov, B. Sandstede, X. J. and Wang, AUTO97: Continuation and bifurcation software for ordinary differential equations, Concordia University, Montreal, 1997.
- [25] G. A. Korn, T. M. Korn, Mathematical Handbook for Scientists and Engineers, Dover Publications, 2000.